



Experimental assessment of the flexural behaviour of circular rubberized concrete-filled steel tubes



A. Silva^a, Y. Jiang^{a,c}, J.M. Castro^{a,*}, N. Silvestre^b, R. Monteiro^c

^a Department of Civil Engineering, Faculty of Engineering, University of Porto, Portugal

^b LAETA, IDMEC, Department of Mechanical Engineering, Instituto Superior Técnico, Universidade de Lisboa, Portugal

^c Istituto Universitario di Studi Superiori di Pavia, Italy

ARTICLE INFO

Article history:

Received 7 January 2016

Received in revised form 11 April 2016

Accepted 13 April 2016

Keywords:

Concrete-filled steel tubes

Rubberized concrete

Monotonic behaviour

Cyclic behaviour

Eurocode 4

Eurocode 8

ABSTRACT

The main objective of the research presented in this paper is to investigate the flexural behaviour of concrete filled steel tube (CFST) columns of circular cross-section, made with rubberized concrete (RuC). A second objective is to identify behavioural differences between this type of composite members and typical CFST members made with standard concrete (StdC), namely in terms of the influence of the rubber aggregate replacement ratio on member strength, ductility, and energy dissipation capacity. The paper describes the preparation and development of an experimental campaign, involving the testing of 16 circular specimens, 12 RuCFST and 4 StdCFST. The definition of the test campaign considered a number of parameters, namely cross-section slenderness, aggregate replacement ratio, axial load level and loading type. A special device was developed as part of an innovative testing setup, aimed at reducing both the cost and preparation time of the specimens. This paper also describes the comparison of the test results with design provisions from Eurocode 4. The test results show a marginal influence of the type of concrete infill on the monotonic and cyclic behaviour of the members and also allow concluding that Eurocode 4 is conservative in predicting the capacity of the tested specimens. Moreover, it is found that the cross-section slenderness does not have a significant influence on the monotonic and cyclic behaviour of the specimens, pointing out for the possible relaxation of the cross-section slenderness limits currently specified in Eurocodes 4 and 8.

© 2016 Elsevier Ltd. All rights reserved.

1. Introduction

In recent years, the use of concrete filled steel tubes (CFSTs) has increased in many modern structures. One of the key benefits of CFSTs is the confinement effect of the concrete provided by the steel tube. Unlike typical reinforced concrete members, CSFT members can make full use of the concrete material as it is fully encased by the steel tube. The tube not only assists in the axial bearing capacity of the member, but also provides confinement to the concrete core. This leads to lighter and more cost efficient solutions than reinforced concrete. Moreover, the triaxial compression stress state of the CFST core can prevent the brittle behaviour of the material. From a structural point of view, the concrete core has the ability to delay local buckling of the steel tube therefore increasing the ductility of the member. Indeed, due to their high ductility and good energy dissipation capacity, CFST members have better performance under seismic loading in comparison with both reinforced concrete and steel tubular elements.

Schneider [1] conducted an experimental and analytical study on the behaviour of short concrete-filled steel tube columns concentrically

loaded in compression up to failure. Fourteen specimens were considered with different cross-section shapes and depth-to-tube wall thickness ratios (d/t and h/t , respectively). The author pointed out that circular steel tubes exhibit much higher post-yield axial ductility than square or rectangular tube cross-sections. Sakino et al. [2] carried out a 5-year research on concrete-filled steel tubular column systems. In the study, a total of 114 specimens of different tube shape, depth-to-tube wall thickness ratio, and concrete strength were fabricated and tested. From the experimental results it was concluded that the difference between the ultimate strength and the nominal squash load of circular CFST columns, which is due to the confinement provided by the concrete, can be estimated as a linear function of the tube yield strength. According to the authors, the concrete can restrain the steel tube wall and delay the occurrence of local buckling. Giakoumelis and Lam [3] tested 15 short CFST columns of circular cross-section under compression, and compared the test results with different design codes. The authors found that Eurocode 4 [4] provides a good prediction of the axial strength of concrete filled steel tube columns.

Regarding the flexural behaviour of CFSTs, Elchalakani et al. [5] performed large deformation monotonic tests on circular concrete-filled steel tubes under pure bending, with diameter-to-thickness ratios, d/t , ranging from 12 to 110. The authors concluded that concrete filling fully prevents local buckling and ovalization of cold-formed steel tubes

* Corresponding author at: Department of Civil Engineering, Faculty of Engineering, University of Porto, Porto, Portugal.

E-mail address: miguel.castro@fe.up.pt (J.M. Castro).

with d/t values between 13 and 40, whereas multiple plastic ripples were observed in the inelastic range for CFSTs with d/t between 74 and 110. Moreover, a close look at the moment–curvature responses presented in [5] allows concluding that the influence of d/t on the monotonic flexural behaviour is not very significant. Additionally, Elchalakani and Zhao [6] performed monotonic and cyclic bending tests, the latter using a constant amplitude loading history, on long CFST members of circular cross-section, with diameter-to-thickness ratios, d/t , ranging from 20 to 162. The results indicated that cyclic loading can have a considerable effect on the strength of circular CFST members, particularly for those made of slender steel tubes. Han [7] utilized, in addition to his test results of CFST members under monotonic bending, the experimental data of a number of research authors on the subject. Through a set of 51 CFST members of circular, square and rectangular cross-section, the author concluded that Eurocode 4 is conservative in predicting the capacity of the test specimens, with an average difference of about 10% between the code and the experimental results. More recently, Jiang et al. [8] performed bending tests on square and rectangular thin-walled CFSTs, with width-to-thickness ratios, h/t , ranging from 50 to 100. The author demonstrated that Eurocode 4 is conservative in predicting the flexural capacity of the test specimens, with an average difference of 9% between the code and the experimental results.

During the last few decades, the application of recycled tire rubber in concrete (RuC, rubberized concrete), has become an important research topic. This technology not only enhances the elastic properties of the concrete, but also allows for scrap rubber re-usage, something very much in line with current global trends of carbon footprint reduction. Although its application to asphalt concrete (RAC, Rubberized Asphalt Concrete) has been introduced in the 60s, with a prominent importance in the USA, RuC is still a recent, but very promising, topic. Typically, the total replacement of normal concrete aggregate, small or coarse, results in a significant reduction in concrete strength, whereas with a reduced rubberized aggregate usage, the sway on concrete strength can be minimal, as shown by Khatib and Bayomy [9]. According to the authors, aggregate replacement ratios should not be higher than 20% of the total aggregate volume. Regarding the behaviour of RuC members, Xue and Shinozuka [10] concluded, through free vibration tests, that the average damping coefficient of RuC columns is higher than that of equivalent normal concrete members. Therefore, the authors concluded about the higher energy dissipation capacity of columns with this type technology, highlighting its potential use as a structural material aimed at the improvement of structural behaviour in seismic areas. The application of this material to CFST members has recently been studied by Duarte et al. [11] for stub columns under compression and by Duarte et al. [12] for stub columns under cyclic bending. The authors highlighted the enhanced ductility of CFSTs with rubberized concrete in comparison to standard concrete. Very recently [13], these authors also developed finite element models to simulate the monotonic behaviour of stub CFST columns with RuC under compression and validated the numerical results through the comparison with experimental values.

From a design perspective, and in addition to the provided methods for the calculation of the resistance of composite columns, Eurocode 4 aims to prevent the development of local buckling through limitation

Table 1
EC4 d/t limits for circular CFSTs (adapted from Eurocode 4).

Type	d/t
Circular	$d/t \leq 90 \times 235/f_y$

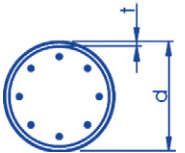
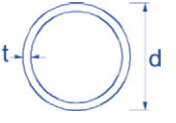


Table 2
EC3 section classification for circular tubes (adapted from Eurocode 3).

Class	d/t
1	$d/t \leq 50 \times 235/f_y$
2	$d/t \leq 70 \times 235/f_y$
3	$d/t \leq 90 \times 235/f_y$



of the cross-section slenderness of the tube, by imposing maximum limits of the d/t ratio, where d is the external diameter of the steel tube and t is the thickness of the tube wall. In this way, the cross-section capacity is expected to be governed by the material properties. For circular members this upper limit is the same as that prescribed in Eurocode 3 [14] for Class 3 tubular steel sections, which effectively indicates that no account is made for the influence of the concrete infill, as shown by the data presented in Tables 1 and 2. Eurocode 8 [15] medium (DCM) and high (DCH) ductility classes for dissipative elements acknowledge the improved CFST behaviour in comparison to the tubular steel section, by presenting more relaxed d/t limits for each ductility class, as illustrated in Table 3, where f_y is the yield strength of the steel tube material. It should be noted that the d/t limits prescribed in Eurocodes 3, 4 and 8 do not make any distinction between the type of internal forces applied to the cross-section (e.g., simple compression, simple bending or combined bending with compression).

It is worth noting that the expressions provided in the current version of Eurocode 8 differ from those provided in Table 3, namely in terms of the coefficient that accounts for the yield stress of the steel. Whilst in Table 3 they are presented in the same format of Eurocodes 3 and 4, i.e. $235/f_y$, in Eurocode 8 they are wrongly presented as $f_y/235$ (Elghazouli and Castro [16]).

This paper mainly focuses on: 1) the experimental assessment of the influence of rubberized concrete (RuC) in CFST members under monotonic and cyclic bending; 2) the comparison of the experimental results with expected design capacities according to Eurocode 4.

2. Description of the Test Campaign

2.1. Specimen Definition

The experimental campaign consisted on the testing of a total of 16 circular CFST columns, 12 with rubberized concrete (RuC) and 4 with standard concrete (StdC), with a free length of 1.35 m, in bending. The considered parameters were the cross-section slenderness ratio d/t , the concrete aggregate replacement ratio β (detailed in Section 2.2.3), the normalized axial load n and the lateral load type. The axial load level n is defined as the ratio between the axial load applied to the specimen and the axial resistance of the cross-section, which was estimated based on the concrete compressive strength and on the available properties of the steel, which were obtained before the cold-forming process. Two levels of axial load were targeted in the test campaign, namely $n = 15\%$ and $n = 0\%$.

In order to study the influence of the cross-section slenderness on member ductility, both high and low values of d/t were considered, taking into account the requirements of Eurocode 8 for high and medium ductility class CFSTs. According to the cross-section slenderness

Table 3
EC8 ductility class requirements for circular tubular sections.

Type	DCM	DCM	DCH
	$1.5 < q \leq 2$	$2 < q \leq 4$	$q > 4$
Steel	EC3 Class 1, 2 or 3	EC3 Class 1 or 2	EC3 Class 1
CFST	$d/t \leq 90 \times 235/f_y$	$d/t \leq 85 \times 235/f_y$	$d/t \leq 80 \times 235/f_y$

Table 4
Specimen list.

Designation	β	Steel tube	Axial load [kN]	Lateral load type
CR-RuC15%-219-3-0%-M	15%	C219 × 3	–	Monotonic
CR-RuC15%-219-3-15%-M			222	
CR-RuC15%-219-3-0%-C			–	
CR-RuC15%-219-3-15%-C		222	Cyclic	
CR-RuC15%-219-5-0%-M		–		
CR-RuC15%-219-5-15%-M		290		
CR-RuC15%-219-5-0%-C	C219 × 5	–	Monotonic	
CR-RuC15%-219-5-15%-C		290		
CR-RuC15%-219-5-0%-C		–	Cyclic	
CR-RuC5%-219-5-0%-M	5%	C219 × 5		–
CR-RuC5%-219-5-15%-M			359	
CR-RuC5%-219-5-0%-C		–	Cyclic	
CR-RuC5%-219-5-15%-C		359		
CR-StdC-219-5-0%-M	0%	C219 × 5	–	Monotonic
CR-StdC-219-5-15%-M			380	
CR-StdC-219-5-0%-C		–	Cyclic	
CR-StdC-219-5-15%-C		380		

limits presented in Table 3 two different steel cross-sections with an external diameter equal to 219 mm were adopted, with a wall thickness of 3 mm and 5 mm, henceforth designated by C219 × 3 and C219 × 5, respectively.

The tested specimens are listed in Table 4, in which the specimen name is a simple concatenation of cross-section type, concrete type, steel tube geometrical properties, axial load level and lateral load type (monotonic or cyclic). For example, a specimen designated CR-RuC5%-219-3-15%-C represents a circular CFST member (CR) with $\beta = 5\%$, with steel tube C219 × 3, with a constant axial load level $n = 15\%$ under cyclic lateral loading (C).

2.2. Specimen and Material Properties

2.2.1. Steel Tube Thickness

In order to assess the variability of cross-sectional dimensions in the test campaign specimens, a measurement of the real steel tube thickness t was carried-out, where a total of 8 thickness measurements per specimen were taken. Fig. 1 depicts an example of these measurements, sequential along the perimeter, for one of both steel section C219 × 3 and C219 × 5 test specimens. The analysis of the examples denotes a relatively high variability in the steel tube thickness. Table 5 summarizes the obtained values for all the specimens of each steel section, in terms of mean of population values, μ , and the corresponding standard deviation, σ .

2.2.2. Steel Properties

All steel tubes used in the test campaign are cold-formed. The steel grade of section types C219 × 3 and C219 × 5 is S235 and S275,

Table 5
Summary of steel tube thickness.

Steel section	μ [mm]	σ
C219 × 3	2.96	0.07
C219 × 5	4.72	0.11

Table 6
Average steel properties of the tubes.

Steel section	f_y [MPa]	f_u [MPa]
C219 × 3	308	373
C219 × 5	393	485

respectively. To evaluate the material mechanical properties, and considering that each tube of the same steel section type comes from the same lot, tensile testing of three steel coupons taken from a set of specimens was performed. Table 6 provides a comparison between the average steel mechanical properties, in terms of steel yield strength, f_y , and ultimate strength, f_u .

Having determined the steel tube mechanical properties, it is now possible to compare the values of d/t , for each steel section, with the prescribed limits of Eurocode 4 and Eurocode 8 for circular CFSTs, shown in Tables 1 and 3, respectively. Table 7 (Eurocode 4) and Table 8 (Eurocode 8) show this comparison for both nominal steel tube properties, taking into consideration the steel grade of the tubes, and the real steel tube properties.

Regarding the limits of Eurocode 4, it is possible to conclude that, when the nominal yield strength is considered, the cross-section slenderness of both tubes is lower than the limit values defined in the code. However, when the real yield stress is considered, the slender cross-section (C219 × 3) exceeds the code limit. This indicates that, according to Eurocode 4, the strength and deformation capacity of the tube may be governed by local buckling effects. This issue will be further discussed later in this paper.

As for the limits of Eurocode 8, the consideration of the nominal yield strength of the steel leads to the classification of the C219 × 3 and C219 × 5 members as of high ductility ($q > 4$). However, when the real steel properties are considered, steel section C219 × 3 does not comply with any of the ductility classes of the code. This observation will be a matter of further discussion in later sections of this paper.

2.2.3. Concrete Properties

Two different ranges of aggregate size were used in order to produce a reference concrete mixture: fine aggregate 0/4 G_F85 and coarse aggregate 4/10 G_C85/20. Two levels of aggregate replacement ratio (β), RuC5% and RuC15%, were used in the test campaign, by substituting only the largest range of aggregate size, 4/10 G_C85/20, with a percentage of the total amount of normal aggregate used in a given mixture. A

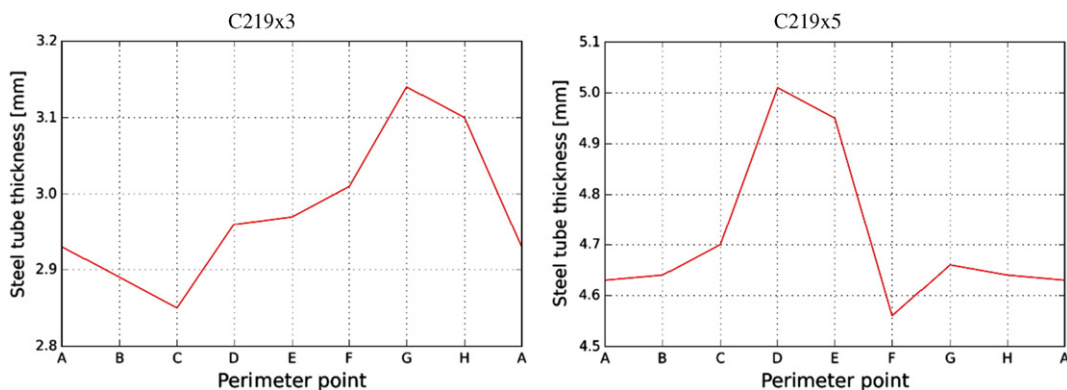


Fig. 1. Steel tube thickness measurement examples.

Table 7
Comparison of d/t of the tubes with the Eurocode 4 limits.

Steel section	Nominal steel properties		Real steel properties	
	C219 × 3	C219 × 5	C219 × 3	C219 × 5
d/t	73.0	43.8	73.0	43.8
f_y [MPa]	235	275	308	393
$90 \times 235/f_y$	90.0	76.9	68.7	53.8

correspondence between the granulometry of the replaced and replacement materials was thus implemented.

In order to determine the concrete mixing ratio of the reference concrete (StdC), the Faury method was used. The rubberized concrete mixtures, RuC5% and RuC15%, were theoretically based on the reference concrete by simple material quantity substitution. However, in order to have the same European slump class S3 of 125 ± 15 mm, determined by lab tests with the Abrams cone across all concrete types, RuC5% and RuC15 have a modified mixing ratio. The obtained mixing ratios for each concrete type are summarized in Table 9. Additionally, the table shows the average cube strength, obtained from the testing of three concrete cubes per mixture, corresponding to the three concrete types used in the test campaign. The tested concrete cubes were taken during steel tube pouring process and tested at 28 days of age. There is a clear influence of the aggregate replacement ratio in the material compressive strength, f_c , which significantly reduces as the amount of normal aggregate that is replaced by rubber aggregates increases.

As the main purpose of the research was to study the difference between the ductile behaviour of RuCFST and CFST, the potential probability of steel tube buckling at a relative low drift should be avoided. Accordingly, C219 × 3 steel tubes were only casted with concrete type RuC15% whereas the C219 × 5 steel tubes were casted with the three concrete types.

2.3. Test Setup

In order to study the behaviour of CFST members in bending, with or without axial load, different setup approaches may be used. In the work carried out by Varma et al. [17], the bottom part of the vertical specimen was fixed to a strong steel base plate, while the top was connected to a vertical actuator, to provide a compression force to the specimen, and to a horizontal actuator that imposed a lateral displacement. One important advantage of such setup is that it can accurately represent the boundary conditions of a CFST member in a structure. However, during the test, a relatively large bending moment develops at the base level, which can cause weld cracking between the specimen and the steel base plate, or cause the steel base plate to yield and have large deformations before the plastic hinge formation in the specimen. In the study of Han et al. [7], the specimen was placed horizontally with two pinned supports at the ends. A horizontal actuator at one of the ends provided the compression force to the specimen, while an actuator at midspan applied a vertical displacement. Specimens under this testing mechanism perform as two cantilevers, separated by the vertical displacement axis. While this avoids the base limitations of the previously mentioned testing setup, it requires greater length specimens to have fully compatible test results.

Table 8
Comparison of d/t of the tubes with the Eurocode 8 limits.

Steel section	Nominal steel properties		Real steel properties	
	C219 × 3	C219 × 5	C219 × 3	C219 × 5
d/t	73.0	43.8	73.0	43.8
f_y [MPa]	235	275	308	393
DCM $90 \times 235/f_y$	90.0	76.9	68.7	53.8
DCM $85 \times 235/f_y$	85.0	72.6	64.9	50.8
DCH $80 \times 235/f_y$	80.0	68.3	61.0	47.8

Table 9
Concrete properties.

	StdC	RuC5%	RuC15%
Water [l/m ³]	216	216	227
Cement [kg/m ³]	420	420	420
0/4 G _r 85 [kg/m ³]	551	551	542
4/10 G _c 85/20 [kg/m ³]	1072	1019	896
Rubber [kg/m ³]	–	54	158
f_c [MPa]	53	39	20

In order to combine the advantages of both types of test setups and reduce the costs associated with the test campaign, a steel box was designed to overcome the aforementioned limitations. As shown in Fig. 2, the box consists of a 1400 × 1400 × 60 mm steel base plate and four steel walls with a height of 500 mm and a thickness of 50 mm welded to each other and to the base plate. Additionally, based on a detailed finite element analysis carried out in ABAQUS [18], five stiffeners were welded on the exterior of each box wall, in order to increase the lateral stiffness of the plates and, consequently, of the testing device. The three stiffeners located in the middle are designed to transfer the lateral force from the steel box to the base plate, while the remaining ones were aimed at receiving the tensile forces and prevent separation between adjacent steel walls, as well as reducing the stress demands imposed on the welds. The internal size of the steel box is 750 × 750 mm, and the base plate is connected to the floor with four Ø25 mm Dywidag rods located at the corners. The internal part of the box has custom made high strength steel bolts and nuts. Each steel bolt is 100 mm long with an additional Ø110 mm hexagon head on one end, to increase the contact area between the bolt and the specimen. Two Ø110 mm steel nuts are used for each steel bolt: one with thickness of 70 mm is welded to the steel wall, to connect with the bolt end, while another with 25 mm is placed between the previous nut and the bolt head, to prevent movement of the bolt during the test. Upon preparation of a specimen, one should position the member in the centre of the steel box; place steel plates between the specimen and the bolts in order to provide proper basal restraint and load transfer; unscrew the bolts until the bolt heads have a full contact with the specimen; and, finally, move the 25 mm nut along the screw until it reaches the steel wall nut. The main drawback of the box is that, due to the layout of the bolts, only rectangular and square specimens can be installed and laterally restrained. Therefore, for circular steel tubes, additional filling steel plates are welded to the bottom part of the tube in order to enable a similar boundary connection to the box constraint mechanism, as shown in Fig. 3. In the test campaign, all the specimens are desired to have a fully restrained base, with vertical and lateral forces applied at the top, as illustrated in Fig. 4.

The specimens were tested under constant axial load and monotonic or cyclic increasing lateral load. Due to the characteristics of the test setup, the specimen test length was approximately 1.35 m. The axial load N_0 was applied on some of the specimens and maintained constant

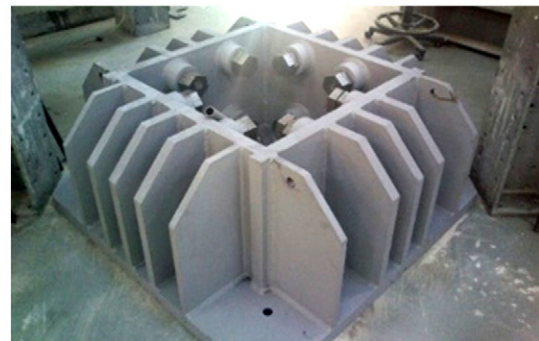


Fig. 2. Designed steel box.



Fig. 3. Circular CFST detail.

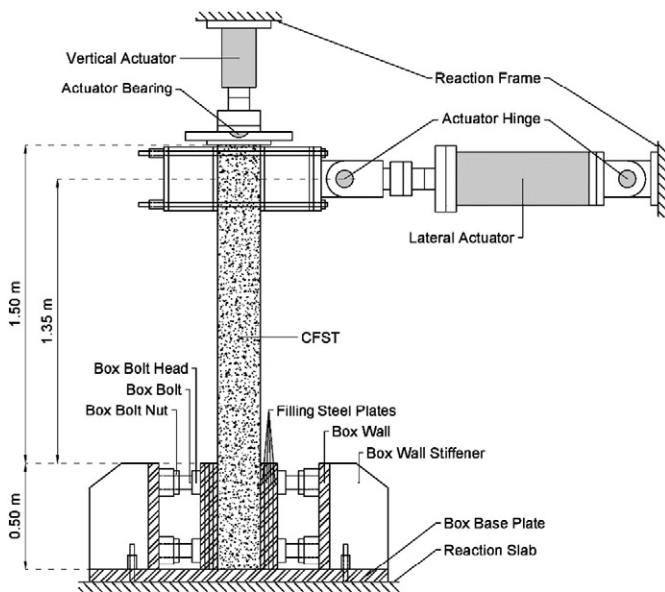


Fig. 4. Test setup.

throughout the test by a 750 kN maximum capacity actuator. The level of axial load was controlled in the lab by a hydraulic system, in order to have a pre-defined axial load in the member. Precautions were made to avoid any eccentricity in the axial load application through a

very precise positioning of the specimen in the box, and to avoid non-uniform axial loading of the member's top cross-section by aligning both the concrete core and the steel tube edges. The lateral loading cyclic protocol was based on the SAC loading protocol [19], as shown in Fig. 5, in which six cycles are imposed for specimen drift ratios $\theta = 0.375\%$, $\theta = 0.50\%$ and $\theta = 0.75\%$, four cycles at $\theta = 1\%$, and two cycles for the remaining levels of θ with 1% increment.

Due to lateral actuator range limitations, displacement levels were limited to a maximum of 300 mm hence, given that the specimen was aligned with the centre of the box, the range of movement of the top of each specimen was between ± 150 mm. This value decreased to ± 70 mm in the tests with applied vertical load, in order to minimize test frame vibrations induced by vertical loads with high lateral displacements, and by some range limitations of the vertical actuator in the lateral direction. The loading capacity of the lateral actuator was limited to a maximum of 500 kN. The imposed lateral displacement was measured by an internal measurement system, and the level of applied force was measured using a load cell. The measurement of the rotation of the bottom cross-section of the specimen at the point of maximum flexural demand during the test, above the 500 mm of box constraints, was made with two inclinometers located on the two sides of the member. These proved to be necessary to take into account the rigid body rotation in the evaluation of the effective top lateral displacement.

Testing was conducted either up to specimen failure, only of significance in cyclic lateral loading, or until the actuator range limits were reached, which are more important in monotonic tests. Only minimal displacements of the box walls top edge were observed in the lateral direction. All the tested specimens showed a very ductile behaviour, and testing proceeded in a smooth and controlled manner.

3. Experimental Results and Specimen Behaviour

3.1. Behaviour of the Testing Device

The development of a new testing device always comes with it a certain degree of concern, as the limitations of its correct applicability are somewhat unknown. To such extent, the test campaign carried out in this research included some level of behavioural control of the mechanism employed to materialize the base restraint. This included monitoring the lateral displacement of the box wall in the direction of the test, using an LVDT (Fig. 6) and the level of rotation above the height of the box constraint, with the use of two inclinometers (Fig. 7). It is important to note that the inclinometers used for this analysis were able to measure, for each side of the specimen, both the rotation about the axes orthogonal (X) and parallel (Y) to the test direction. These are, in fact, the rotations of the unconstrained base of the specimen during the test, above the height of the filling steel plates.

Regarding the deformation of the box walls, as expected, a linear correlation between the stiffness of the tested specimen and the level of displacement of the box wall was found. Indeed, the observed peak displacement was higher for the test specimens with the steel tube C219 × 5 than for those with C219 × 3, and increased linearly while the specimen was in the elastic range, remaining constant after the formation of a plastic hinge in the member. Although present, this level of displacement was negligible and unnoticeable during the test,

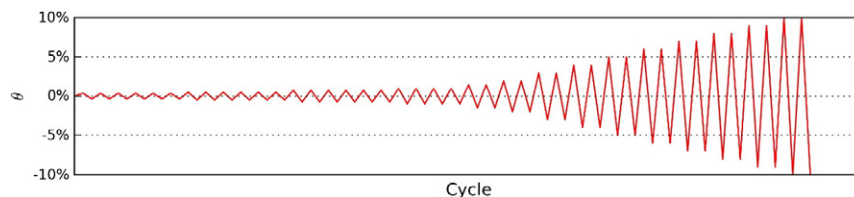


Fig. 5. Cyclic loading protocol.

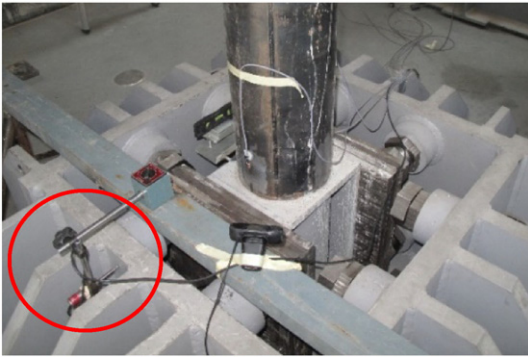


Fig. 6. LVDT positioning at one of the box walls.

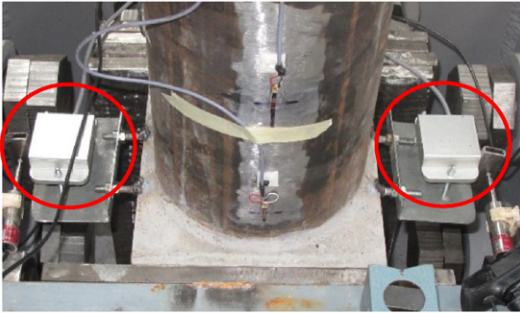


Fig. 7. Inclinometer positioning at the specimen's base.

as confirmed by Fig. 8, where the level of box wall deformation is significantly lower than the level of imposed displacement.

As for the base rotations, the test results presented in Fig. 9, taken for each specimen and for rotations X and Y as the average measurements between both inclinometers, demonstrate similar trends to those observed for the box wall deformation. Interestingly, a correlation between the specimen's base X rotation and the level of imposed lateral force was found, where both values are proportional by the same factor throughout the test. It was however found that, in order to have accurate results for the level of imposed lateral displacement at the top of the composite column, a correction should be made regarding the displacement component related with X rotation. On the other hand, no significant influence of Y rotation in the test results was found. Therefore, for each test, the “real” imposed lateral displacement is given by $\Delta^{real} = \Delta - X \cdot h$, where Δ is the imposed lateral displacement, X is the rotation, and h the clear height of the test specimen, taken as 1.35 m.

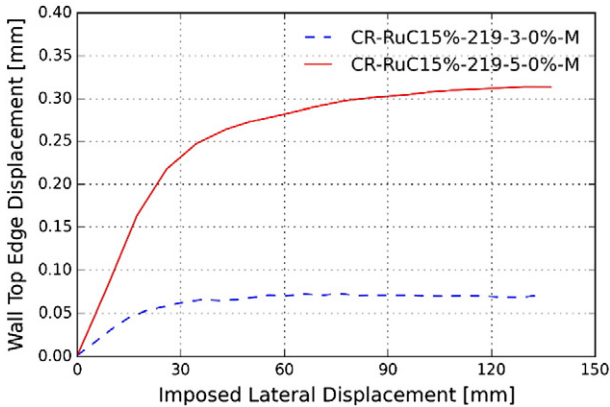


Fig. 8. Box wall displacement for test specimens CR-RuC15%-219-3-0%-M and CR-RuC15%-219-5-0%-M.

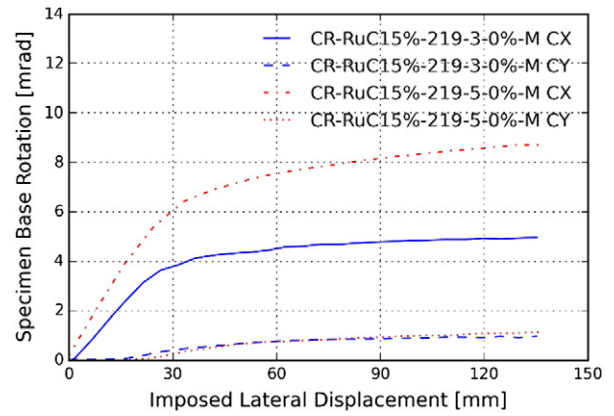


Fig. 9. Average base rotations for test specimens CR-RuC15%-219-3-0%-M and CR-RuC15%-219-5-0%-M.

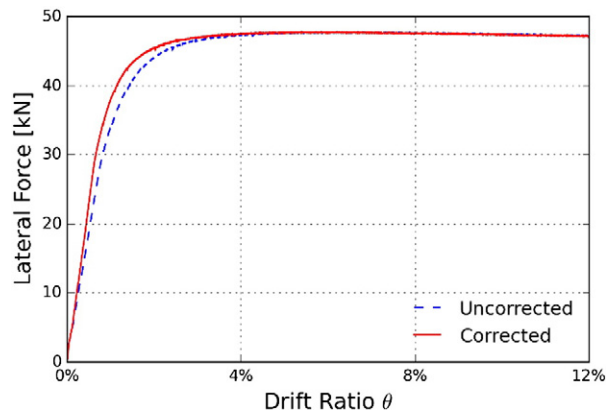


Fig. 10. Δ^{real} correction for test specimen CR-RuC15%-219-3-0%-M.

Figs. 10 and 11 illustrate this displacement correction for test specimens CR-RuC15%-219-3-0%-M and CR-RuC15%-219-5-0%-M, respectively.

The procedure used for the base rotation measurement proved to be a noteworthy advantage of the developed testing device, as it is easier to implement than with the typical steel only testing setup, where the steel section is welded at the base to a very thick plate, which in turn is connected to the reaction floor. In the latter case, the specimen's base rotation that can occur during the test, for example due to buckling of the base plate, is measured indirectly with LVDTs, adding a level of complexity and inaccuracy to the procedure.

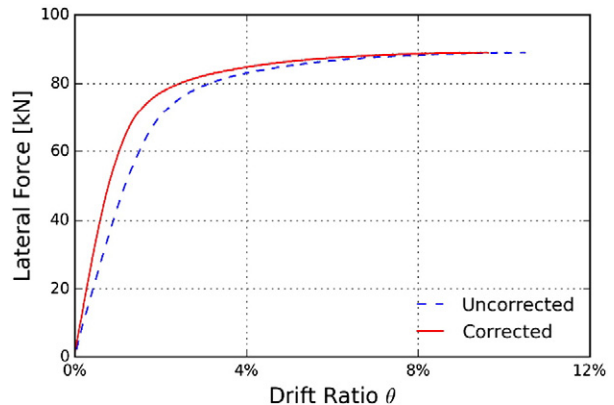


Fig. 11. Δ^{real} correction for test specimen CR-RuC15%-219-5-0%-M.



Fig. 12. Local buckling of the steel tube in a monotonic test.



Fig. 13. Fracture of the steel tube during a cyclic test.

3.2. Test Results

In all the specimens tested under monotonic lateral loading, combined or not with a constant axial load, a typical local plastic mode consisting of outward buckling was observed. However, even for the large levels of drift ratio reached in the tests, the level of buckling deformation was relatively low. As far as the cyclic lateral loading tests are concerned, all specimens without axial loading exhibited a failure mode characterized by fracture of the steel section after very significant local buckling of the tube wall, with a clear influence on the global behaviour of the specimen. Figs. 12 and 13 show the yield mechanism and failure mode for monotonic and cyclic lateral loading, respectively.

Fig. 14 to Fig. 21 show the test results for all the circular specimens tested in the campaign, where, in general, all members exhibited a very ductile behaviour. It can be seen that strength degradation only occurred for drift ratios higher than 4 to 5%. In the figures, the results are presented as a function between the applied lateral force and

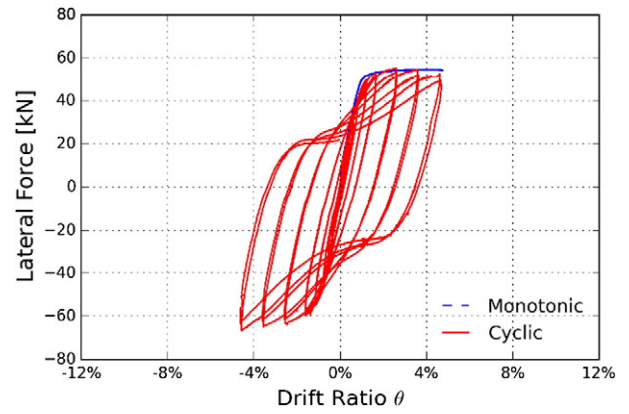


Fig. 15. Test results for CR-RuC15%-219-3-15% specimens.

the corresponding specimen's drift ratio, θ , obtained by dividing the member's "real" top lateral displacement by the clear height of 1.35 m.

For the monotonic tests without axial load, it was found that, despite the levels of column drift close to $\theta = 10\%$, loss of lateral force resistance either did not occur or was insignificant. However, for the corresponding cyclic test, the effect of considerable local buckling in the member's plastic hinge region was responsible for the decrease of lateral resistance for increasing levels of deformation. Across all cyclic test results, it is clear at which stage during the test the member's local deformation went from substantial local buckling to fracture, where a noteworthy

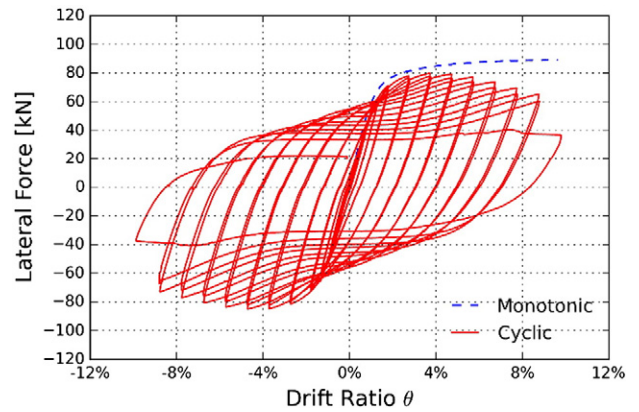


Fig. 16. Test results for CR-RuC15%-219-5-0% specimens.

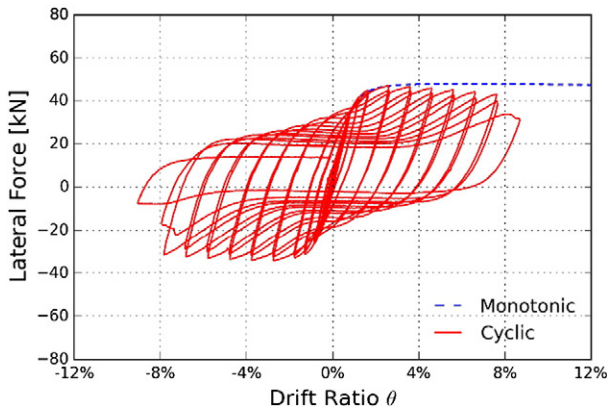


Fig. 14. Test results for CR-RuC15%-219-3-0% specimens.

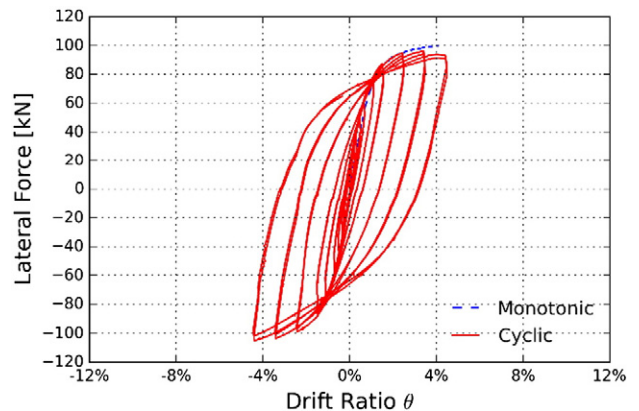


Fig. 17. Test results for CR-RuC15%-219-5-15% specimens.

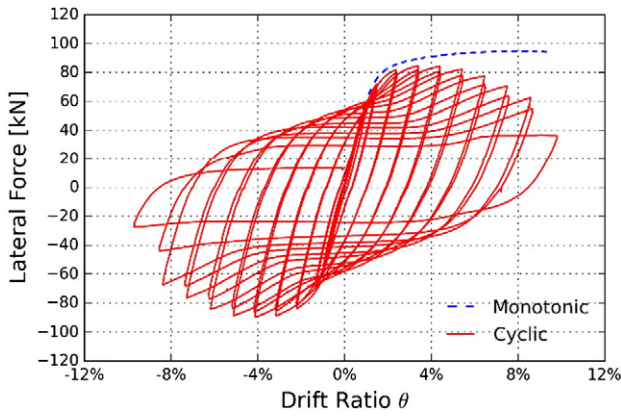


Fig. 18. Test results for CR-RuC5%-219-5-0% specimens.

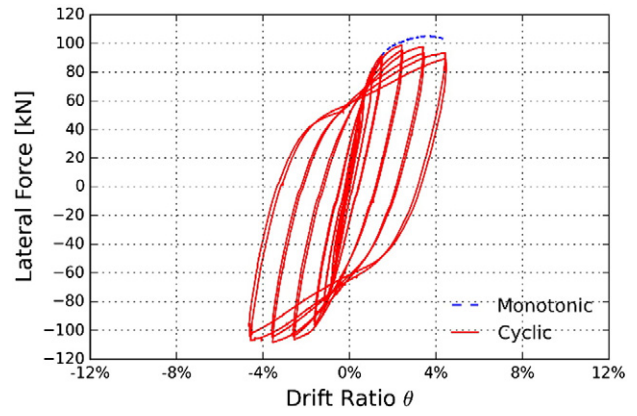


Fig. 21. Test results for CR-StdC-219-5-15% specimens.

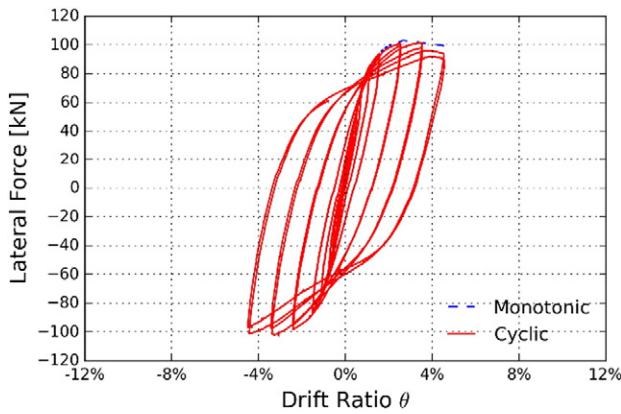


Fig. 19. Test results for CR-RuC5%-219-5-15% specimens.

loss of lateral force strength is found in the last few cycles, as well as a somewhat irregular behaviour in some of the specimens.

Columns tested with axial loads showed similar behaviour, apart from a significant member strength increase in comparison to the corresponding test without axial load. The former observation can be explained by the tensile cracking inhibition of the concrete that is caused by the compressive axial force, thus enhancing its flexural resistance, or even by some confinement effect of the concrete core not present in a simple bending scenario without axial compression. Due to the lower levels of drift applied, fracture was not observed for these specimens.

3.3. Influence of Steel-section Infill

In CFST members, the concrete core has the ability to significantly improve the behaviour of the member, both in terms of overall strength and ductility. In the test campaign, one circular C219 × 3 hollow steel specimen was tested under monotonic lateral loading without an applied axial force, in order to gauge the improvement in member behaviour induced by the section concrete infill. A member compatible with test specimen CR-RuC15%-219-3-0%-M was used. Fig. 22 shows the global force-deformation curve of both specimens, and Figs. 23 and 24 show the local deformation mode of the steel and CFST specimens, respectively, at the final stage of the experiment. The results are

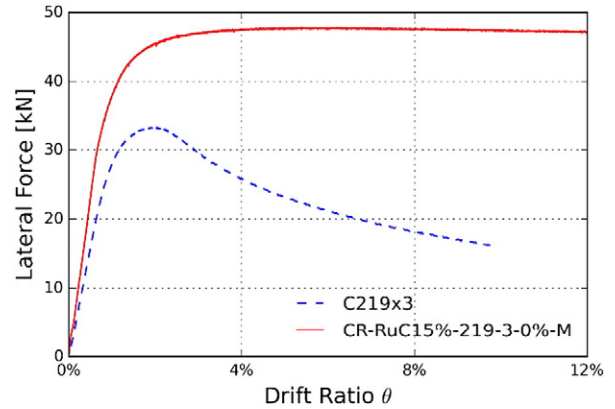


Fig. 22. Monotonic behaviour of steel and CFST specimens.

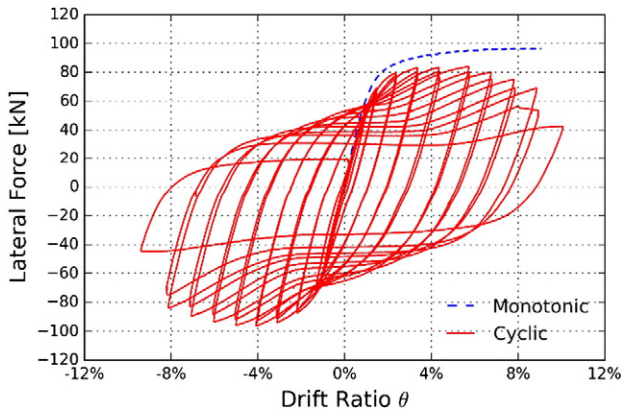


Fig. 20. Test results for CR-StdC-219-5-0% specimens.



Fig. 23. Local buckling of steel specimen C219 × 3.



Fig. 24. Local buckling of RuCFST specimen CR-RuC15%-219-3-0%-M.

summarized in Table 10 where the values of specimen elastic stiffness, K , maximum lateral force, F_{max} , and the corresponding level of drift ratio, $\theta_{F_{max}}$, are calculated and compared.

When analysing the deformed shape of the local buckling modes, no significant differences in buckle amplitude can be identified. However, it was clear during the tests that this maximum amplitude was reached for higher levels of imposed top displacement in the case of the composite specimen. Interestingly, by examining the monotonic test curves, it can be seen that in spite of the local buckling mechanisms developed in both specimens, only in C219 × 3 this effect had a pronounced influence on the global behaviour of the member. Specimen C219 × 3 exhibited significant strength degradation after reaching the maximum lateral applied force, in comparison to that of CR-RuC15%-219-3-0%-M for which load degradation was minimal. Furthermore, substantial improvements in monotonic behaviour are evident due to composite action, with an increase of 43% in the peak lateral force, 32% in the corresponding level of drift, and 89% in the elastic stiffness.

3.4. Influence of Concrete Type

In order to assess the influence of the concrete type on member behaviour, some comparisons between equivalent test specimens are now carried out. Since only one of the circular steel sections, C219 × 5, was considered to have three types of concrete cores, the test results obtained for this type of specimen will be used for the sake of comparison. In the following paragraphs, this assessment is carried out in terms of type of lateral loading, i.e. monotonic or cyclic, and for the different axial load levels, n , considered in the test campaign.

3.4.1. Monotonic Loading

Regarding the specimens tested under monotonic lateral loading, with and without axial load, it can be seen in Figs. 25 and 26 that the column behaviour is not significantly affected by the concrete type. Moreover, the comparisons between the members with standard concrete, StdC, and 5% rubberized concrete, RuC5%, show slight differences only for the final stages of deformation, despite the 20% reduction of the concrete strength, f_c , from StdC to RuC5%. When comparing the test specimens CR-StdC-219-5 and CR-RuC15%-219-5, the 60% decrease in f_c does not reflect in significant loss of lateral resistance. A summary of specimen behaviour is presented in Table 11 where the values of maximum lateral force, F_{max} , and the corresponding level of drift ratio, $\theta_{F_{max}}$, are determined and compared with the results obtained for the CR-StdC-219-5 specimen.

Table 10

Influence of steel section infill on specimen monotonic behaviour.

Specimen	K [kN/m]	K/K_{Steel}	F_{max} [kN]	$F_{max}/F_{max, Steel}$	$\theta_{F_{max}}$	$\theta_{F_{max}}/\theta_{F_{max, Steel}}$
C219 × 3	1793	–	33.3	–	1.95%	–
CR-RuC15%-219-3-0%-M	3394	1.893	47.8	1.434	5.38%	1.319

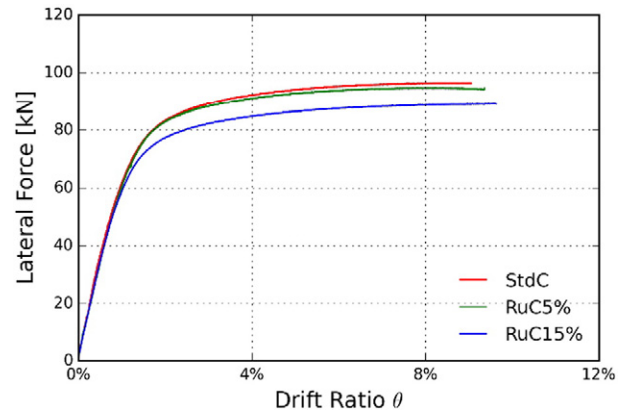


Fig. 25. Monotonic test results of CR-219-5 for $n = 0\%$.

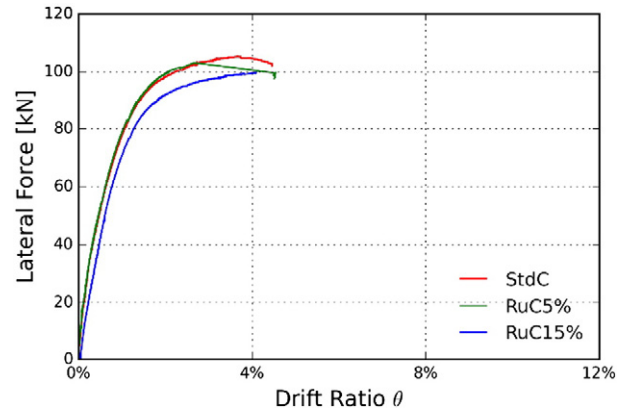


Fig. 26. Monotonic test results of CR-219-5 for $n = 15\%$.

Table 11 demonstrates that the behavioural differences between specimens are minimal. The reduction in maximum lateral force of specimens with RuC5% ranges from 0.2 and 1.8%, and with RuC15% from 5.3 to 7.7%, in spite of a corresponding reduction of 20% and 60% of the concrete compressive strength. Therefore, it can be concluded that the flexural behaviour of circular CFST columns subjected to monotonic loading mostly depends on the properties of the steel tube, as significantly different concrete cores have practically no influence on the specimen's behaviour.

3.4.2. Cyclic Loading

The results for specimens tested under cyclic lateral loading with both axial load levels, n , shows once again that the concrete type has very limited influence column behaviour, which is in agreement with the results obtained for monotonic tests, as shown in Figs. 27 and 28. Furthermore, by comparing StdC with the remaining case study types, no significant differences in specimen behaviour are found. Notwithstanding the slight reductions of maximum lateral force, in line with the results obtained for monotonic loading, the influence of aggregate replacement ratio in member ductility proves to be marginal. As in Section 3.4.1., a summary of specimen behaviour is presented in Table 12, where the values of maximum lateral force, F_{max} , and the

Table 11
Influence of concrete type on the monotonic behaviour.

Specimen	F_{max} [kN]	$F_{max}/F_{max,StdC}$	$ \theta_{F_{max}} $	$\theta_{F_{max}}/\theta_{F_{max,StdC}}$
CR-StdC-219-5-0%-M	96.5	–	9.01%	–
CR-RuC5%-219-5-0%-M	94.8	0.982	8.39%	0.931
CR-RuC15%-219-5-0%-M	89.1	0.923	8.96%	0.995
CR-StdC-219-5-15%-M	105.3	–	3.66%	–
CR-RuC5%-219-5-15%-M	105.6	1.002	3.18%	0.869
CR-RuC15%-219-5-15%-M	99.7	0.947	4.08%	1.115

corresponding level of drift ratio, $\theta_{F_{max}}$, are calculated and compared with the reference CR-StdC-219-5 specimen.

The analysis of the results presented in Table 12 caters for conclusions regarding some differences in the performance of the analysed specimens. The decrease in maximum lateral force of RuC5% specimens is close to 7%, and with RuC15% ranges from 4.4 to 11.5%, despite a corresponding decrease of 20% and 60% of concrete strength. These observations denote, and in line with the conclusions obtained from the monotonic tests, a very minor influence of concrete infill type on member behaviour. It is important to note that the same does not occur for axial compression loading scenarios, in which concrete strength has an important influence on the axial strength of CFST members. This difference can be explained by the mechanism of internal forces that develops in the cross-section. Whilst in a CFST subjected to simple compression the axial resistance of the cross-section results from a contribution of the two materials (concrete and steel), proportional to the area and compressive strength of each material, the same does not occur for flexural imposed loading. With the development of a plastic moment in the cross-section, the position of the neutral axis is such that only a small portion of the concrete part effectively contributes to the flexural capacity (concrete strength in tension is minimal and thus may be disregarded). Conversely, if local buckling does not occur, the steel tube part is able to develop yield stresses in the whole section. This difference between material contributions, in addition to the significant difference between concrete and steel yield strength

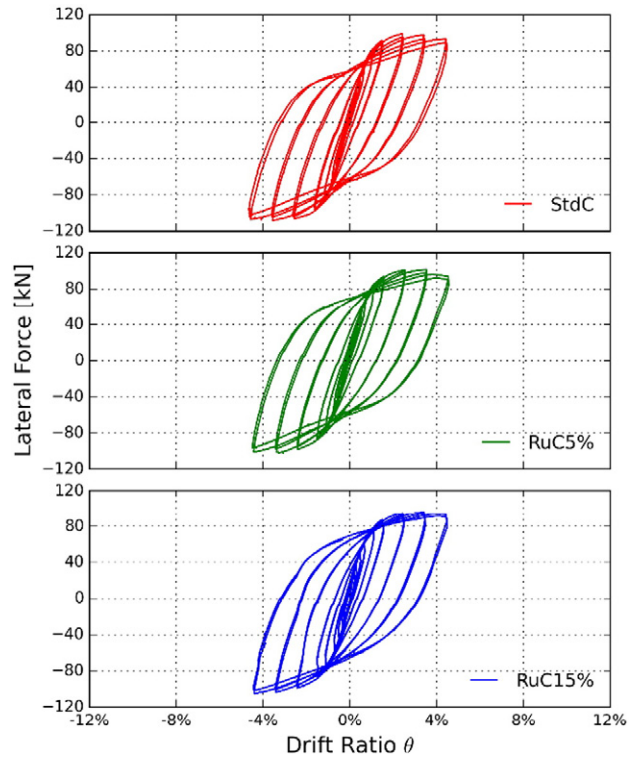


Fig. 28. Cyclic test results of CR-219-5 for $n = 15\%$.

(usually with a ratio higher than 10), results in a value of flexural strength of the member that is largely dominated by the contribution of the steel tube.

3.5. Influence of Loading Type

The behaviour of structural members subjected to monotonic loading may feature noticeable differences with respect to cyclic loading, both in terms of strength and ductility hence a comparison is now carried out in order to assess the influence of the loading type on the member behaviour. Table 13 summarizes the peak lateral load measured during the experimental test, F_{max} , as well as the corresponding level of specimen drift ratio, $\theta_{F_{max}}$. The analysis of the obtained results leads to the conclusion that influence of the nature of the applied lateral load on specimen deformation capacity is relevant.

Regarding the specimens tested under simple bending, changes in specimen strength were found, namely higher strengths on monotonic tests in comparison to cyclic tests. This observation reflects the development of local buckling at the base of the specimens, which was significant in the cyclic tests and minimal in the specimens tested monotonically. However, this observation changed in the case of the specimens tested under combined bending with compression, where the peak lateral load was higher for the cyclic tests with respect to the monotonic counterpart. A possible explanation for this observation may be found on material cyclic hardening. The presence of a constant

Table 12
Influence of concrete type on the cyclic behaviour.

Specimen	$ F_{max} $ [kN]	$F_{max}/F_{max,StdC}$	$ \theta_{F_{max}} $	$\theta_{F_{max}}/\theta_{F_{max,StdC}}$
CR-StdC-219-5-0%-C	96.3	–	4.08%	–
CR-RuC5%-219-5-0%-C	89.8	0.932	4.12%	1.010
CR-RuC15%-219-5-0%-C	85.2	0.885	4.70%	1.152
CR-StdC-219-5-15%-C	110.2	–	3.41%	–
CR-RuC5%-219-5-15%-C	102.7	0.933	3.07%	0.900
CR-RuC15%-219-5-15%-C	105.3	0.956	4.36%	1.281

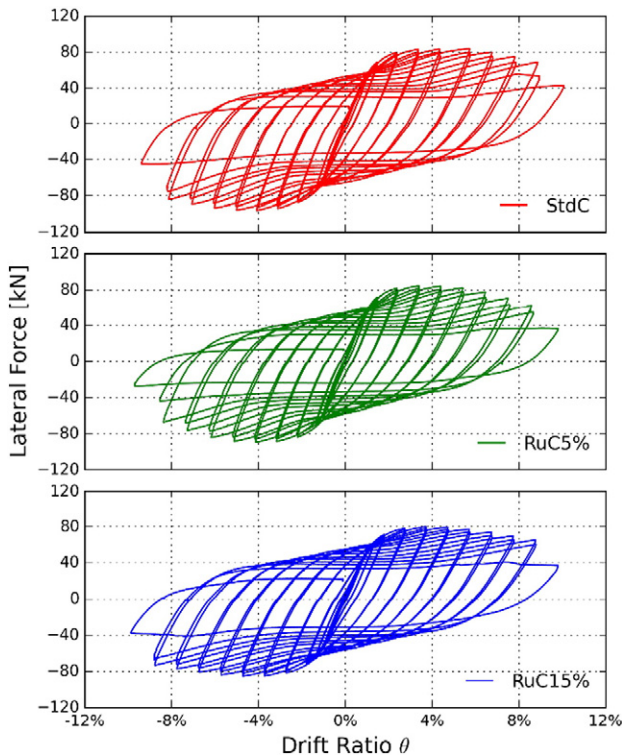


Fig. 27. Cyclic test results of CR-219-5 for $n = 0\%$.

Table 13
Influence of loading type on specimen's behaviour.

Specimen	$ F_{max} $ [kN]	F_{max}^M/F_{max}^C	$ \theta_{F_{max}} $	$\theta_{F_{max}}^M/\theta_{F_{max}}^C$
CR-RuC15%-219-3-0%-M	47.8	1.024	5.38%	2.099
CR-RuC15%-219-3-0%-C	46.7		2.56%	
CR-StdC-219-5-0%-M	97.7	1.015	9.01%	2.210
CR-StdC-219-5-0%-C	96.3		4.08%	
CR-RuC5%-219-5-0%-M	95.4	1.064	8.39%	2.038
CR-RuC5%-219-5-0%-C	89.7		4.12%	
CR-RuC15%-219-5-0%-M	90.7	1.065	8.96%	1.908
CR-RuC15%-219-5-0%-C	85.2		4.70%	
CR-RuC15%-219-3-15%-M	54.8	0.822	4.26%	0.936
CR-RuC15%-219-3-15%-C	66.7		4.55%	
CR-StdC-219-5-15%-M	105.3	0.956	3.66%	1.073
CR-StdC-219-5-15%-C	110.2		3.41%	
CR-RuC5%-219-5-15%-M	105.6	1.028	3.18%	1.036
CR-RuC5%-219-5-15%-C	102.7		3.07%	
CR-RuC15%-219-5-15%-M	99.7	0.947	4.08%	0.934
CR-RuC15%-219-5-15%-C	105.3		4.36%	

axial load applied to the member results in earlier yielding of the specimen hence on the development of larger levels of strains in the steel fibres in compression for a given imposed deformation to the specimen, differently from a simple bending case. This justification is not verified for specimen CR-RuC5%-219-5, where the peak lateral force is higher for the monotonic loading type. Such exception may be due to the positioning of the specimen longitudinal weld, resulting from the manufacturing process, as well as the high variability of the test tube thickness.

Regarding the level of specimen drift ratio corresponding to the peak lateral force, $\theta_{F_{max}}$, the results for simple bending show an important decrease going from monotonic to cyclic tests, as the value of drift corresponding to the peak load is, on average, halved. This can also be explained by a greater presence of local buckling of the steel tube on the specimens subjected to cyclic loading. Yet, when combined with axial compression, $\theta_{F_{max}}$ variations are minimal, mainly due to the test being conditioned to lower values of lateral displacement than for simple bending, meaning that the monotonic test may not have reached the peak specimen capacity.

3.6. Influence of Cross-section Slenderness

In order to evaluate the influence of CFST cross-section slenderness on member behaviour, a number of comparisons between test specimens can be made. To that regard, only specimens of steel sections C219 × 3 and C219 × 5, with infill RuC15%, have comparable test results. In the following, this assessment is carried out to for the two types of lateral loading and the different normalized axial load levels n of the test campaign.

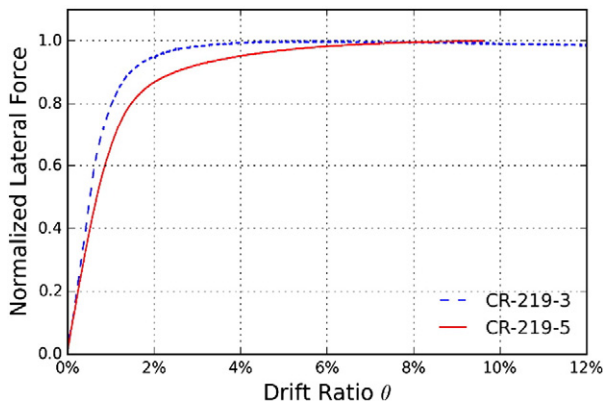


Fig. 29. Monotonic test results of CR-RuC15%-219 for $n = 0\%$.

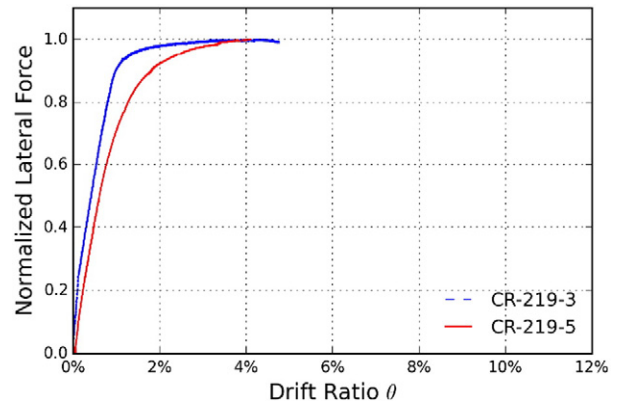


Fig. 30. Monotonic test results of CR-RuC15%-219 for $n = 15\%$.

3.6.1. Monotonic Loading

Concerning the monotonically loaded specimens, regardless of the axial load level, test results show some influence of cross-section slenderness on the member's overall behaviour, as shown in Figs. 29 and 30. The lower value of d/t , corresponding to C219 × 5 specimens, leads to a relative improvement of the ductility of the member. However, for each level of normalized axial load, both specimens exhibited similar ductility. Taking into consideration the d/t limit of Eurocode 4 for circular CFSTs and the comparison shown in Table 7, it is possible to conclude that the specimens exhibited a good behaviour, even though they did not respect the cross-section slenderness limit defined in the European code.

3.6.2. Cyclic Loading

The influence of the cross-section slenderness on the cyclic behaviour of the specimens is shown in Figs. 31 and 32. For the simple bending cases, despite the asymmetry of the force-deformation curve of the slender specimen, the hysteretic behaviour of both specimens was similar for what concerns pinching and degradation effects. It is worth noting that a stable behaviour was observed up to levels of lateral drift ratio of about 7%. Concerning the specimens subjected to combined compression with bending, the test results indicate the presence of pinching effects for the specimen with slender cross-section (C219 × 3 tube), whilst no pinching was observed for the more compact member. Strength degradation was minimal for the range of drift ratios (up to 4%) imposed during the tests.

The results presented above clearly demonstrate that the influence of cross-section slenderness is not as significant as one could infer from the d/t limits prescribed in Eurocode 8 (Table 8) where the slenderness limits that distinguish between high and moderate ductile members are very close. As showed in Table 8, the members under investigation are classified with very different ductility properties

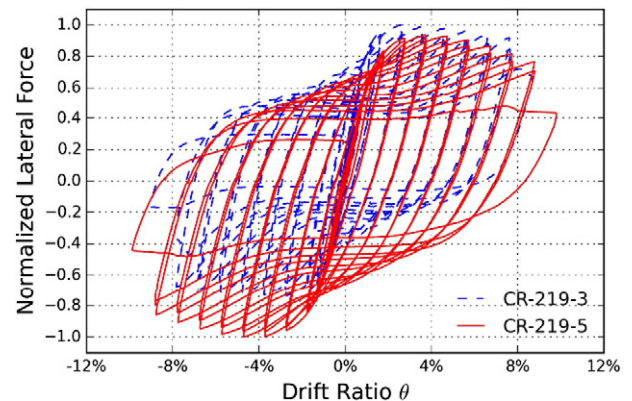


Fig. 31. Cyclic test results of CR-RuC15%-219 for $n = 0\%$.

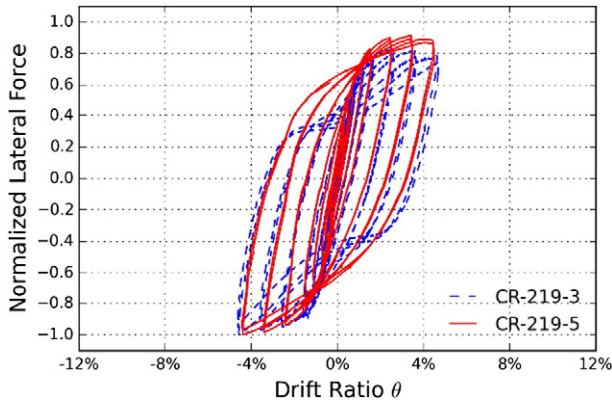


Fig. 32. Cyclic test results of CR-RuC15%-219 for $n = 15\%$.

however, taking into consideration the experimental results obtained, the differences in ductility observed were not significant. It is important to note that, although the columns with steel tube $C219 \times 3$ exceed the d/t requirements of Eurocode 8, when the real yield strength of the tubes is taken into account, the specimens exhibited a good hysteretic behaviour up to significant levels of lateral deformation. These observations clearly point towards a possible relaxation of the cross-section slenderness limits defined in Eurocode 8.

4. Design Comparisons

4.1. Design Calculation Procedure of Eurocode 4

According to Eurocode 4 (EC4), the cross-sectional resistance of a composite column under uniaxial bending, M , with or without axial compression, N , can be determined from an interaction curve $N - M$, as illustrated in Fig. 33. The points defining this curve can be determined by considering different plastic neutral axis positions in the principal bending plane under consideration. By assigning plastic stress blocks, together with the two equations of equilibrium, the combined values of moment and axial resistances are obtained. EC4 defines a methodology for the calculation of a simplified interaction curve AECDB (Fig. 33).

For CFST members with circular hollow sections (CHS), the plastic axial resistance, $N_{pl,Rd}$, may take into account the confinement effect, provided that $\bar{\lambda} = \sqrt{N_{pl,Rk}/N_{cr}} < 0.5$, where $\bar{\lambda}$ is the normalized slenderness, and $e/d < 0.1$, where e is the eccentricity of loading given by M_{Ed}/N_{Ed} and d is the column's external diameter. For CFST members, $N_{pl,Rk} = A_a f_{yk} + A_c f_{ck}$, where A_a and A_c are the cross-section areas of the steel tube and concrete core, respectively, and f_{yk} and f_{ck} denote the characteristic values of the steel yield strength and concrete compressive strength, respectively.

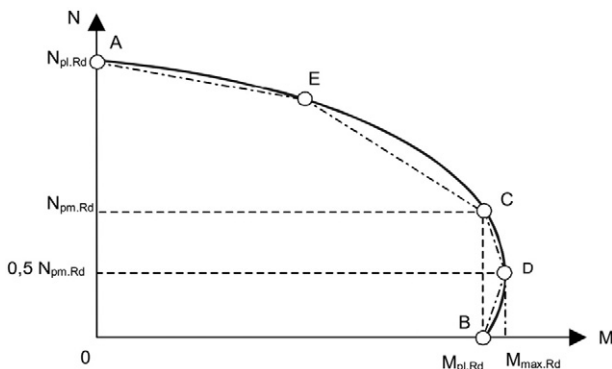


Fig. 33. Interaction curve $N - M$ with EC4 linear approximation (adapted from Eurocode 4).

Table 14

Parameter η for the calculation of plastic resistance to axial force.

$e/d = 0$	$0 < e/d \leq 0.1$	$e/d > 0.1$
$\eta_a = \eta_{ao} = 0.25(3 + 2\bar{\lambda}) \leq 1.0$	$\eta_a = \eta_{ao} + (1 - \eta_{ao})(10e/d)$	$\eta_a = 0$
$\eta_c = \eta_{co} = 4.9 - 18.5\bar{\lambda} + 17\bar{\lambda}^2 \geq 0$	$\eta_c = \eta_{co}(1 - 10e/d)$	$\eta_c = 0$

Axial resistance, $N_{pl,Rd}$, is determined as $N_{pl,Rd} = \eta_a A_a f_{yd} + (1 + \eta_c \frac{t}{d} \frac{f_y}{f_{ck}}) A_c f_{cd}$, where the steel tube and the concrete core yield strengths are calculated with the respective partial safety factors, and their contributions are affected by the parameter η , which depends on the confinement conditions described in the previous paragraph and summarized in Table 14. One can easily conclude that no confinement effect can be accounted for in the case of bending without axial compression, as the ratio e/d is infinite hence higher than 0.1.

For CFST columns, the point C of the interaction is given by $N_{pm,Rd} = A_c f_{cd}$. In the case of the bending moment coordinate, $M_{pl,Rd}$, the height of the neutral axis h_n must be determined, assuming a totally plastic stress block distribution and no contribution from the concrete in tension, with cross-sectional static equilibrium. As points B and C are associated to the same value of bending moment, the procedure for the calculation of $M_{pl,Rd}$ for circular columns in point B of the simplified interaction curve, i.e. without an applied axial force, is shown in the following, adopting the terminology shown in Fig. 34.

For circular CFSTs, the calculation of h_n follows Eq. (4.1), which simply establishes the equilibrium of forces at the cross-section. The second equilibrium equation, i.e. of zero bending moment sum, is used to calculate $M_{pl,Rd}$ and follows Eq. (4.6). Variables d_{cc} , d_{ac} , $d_{at,i}$ and $d_{at,ii}$ are the vertical distances from the horizontal symmetry axis to the respective centroid of each cross-section element in Fig. 34. It is important to note that this calculation procedure assumes a plastic stress distribution, which is only applicable to behaviour scenarios in which there is no development of local buckling of the steel tube walls. As such, the expressions are not valid for very slender CSFTs, given their potential for the development of relevant local buckling effects. Taking into consideration that Eurocode 4 specifies a limit value of d/t ($90 \times 235/f_y$) so that local buckling effects may be neglected, the application of the following expressions for members that violate this cross-section slenderness limit should be made with caution or, eventually, using a different procedure which will not be focus of discussion in this paper. Nevertheless, as already mentioned before, it is important to note that the slenderness limit defined in the European code is independent of the type of internal forces and hence may be conservative for members subjected mainly to bending conditions.

$$A_a c f_{yd} + A_c c f_{cd} - A_{at,i} f_{yd} - A_{at,ii} f_{yd} = 0 \rightarrow h_n \quad (4.1)$$

where:

$$A_{cc} = \frac{(0.5(d-2t))^2}{2} \times \left[2 \cos^{-1} \left(\frac{h_n}{0.5(d-2t)} \right) - \sin \left(2 \cos^{-1} \left(\frac{h_n}{0.5(d-2t)} \right) \right) \right] \quad (4.2)$$

$$A_{cc} = \frac{(0.5d)^2}{2} \times \left[2 \cos^{-1} \left(\frac{h_n}{0.5d} \right) - \sin \left(2 \cos^{-1} \left(\frac{h_n}{0.5d} \right) \right) \right] - A_{cc} \quad (4.3)$$

$$A_{at,ii} = \frac{\pi(d^2 - (d-2t)^2)}{8} \quad (4.4)$$

$$A_{at,i} = A_{at}^{ii} - A_{cc} \quad (4.5)$$

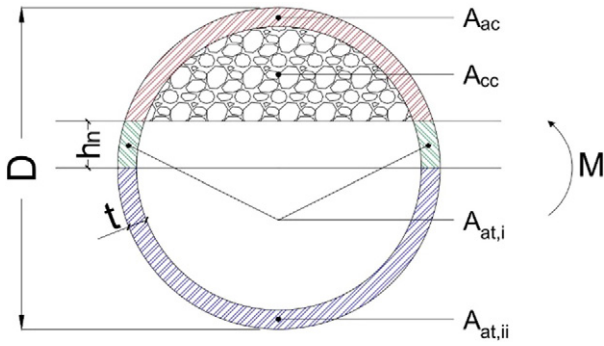


Fig. 34. Circular CFST $M_{pl,Rd}$ calculation procedure.

$$M_{pl,Rd} = A_{ac}f_{yd}d_{ac} + A_{cc}f_{cd}d_{cc} - A_{at,i}f_{yd}d_{at,i} + A_{at,ii}f_{yd}d_{at,ii} \quad (4.6)$$

where:

$$d_{cc} = \frac{2 \times (d-2t) \sin^3 \left(\cos^{-1} \left(\frac{h_n}{0.5(d-2t)} \right) \right)}{3 \times \left[2 \cos^{-1} \left(\frac{h_n}{0.5(d-2t)} \right) - \sin \left(2 \cos^{-1} \left(\frac{h_n}{0.5(d-2t)} \right) \right) \right]} \quad (4.7)$$

$$d_{ac} = \frac{(A_{ac} + A_{cc}) \frac{2d \times \sin^3 \left(\cos^{-1} \left(\frac{h_n}{0.5d} \right) \right)}{3 \left[2 \cos^{-1} \left(\frac{h_n}{0.5d} \right) - \sin \left(2 \cos^{-1} \left(\frac{h_n}{0.5d} \right) \right) \right]} - A_{cc}d_{cc}}{A_{ac}} \quad (4.8)$$

$$d_{at,ii} = \frac{\frac{d^3 - (d-2t)^3}{12}}{A_{ac,ii}} \quad (4.9)$$

$$d_{at,i} = \frac{A_{at,ii}d_{at,ii} - A_{ac}d_{ac}}{A_{at,i}} \quad (4.10)$$

Finally, the value of $M_{max,Rd}$, corresponding to point D of the interaction curve is given by Eq. (4.11), where W_{pla} and W_{plc} are the plastic section modulus of the steel tube and concrete core, respectively.

$$M_{max,Rd} = W_{pla}f_{yd} + 0.5W_{plc}f_{cd} \quad (4.11)$$

4.2. Results and Discussion

Taking into account the aforementioned procedures for the calculation of the bending capacity of circular CFST members, it is possible to assess the accuracy of EC4 in predicting the strength of the composite specimens that were tested in the experimental campaign. These comparisons can only be achieved for the monotonic test results, as no consideration is given in the code to behavioural differences in cyclic loading. Moreover, given that only two levels of axial loading were considered, $n = 0$ and $n = 15\%$, only two points of the interaction curve can be used for comparison, one of them being point B (Fig. 33) in the case of simple bending.

The evaluation of Eurocode 4 provisions should be made by comparing the design bending moment with the corresponding value from the test. However, this procedure proved to be difficult to implement, given the complexity associated with the estimation of the yield moment measured from the experimental tests. Therefore, the following evaluation is shown as the comparison between the obtained maximum bending moment in the test, M_u^{TEST} , given by the multiplication of the maximum applied lateral force, F_u^{TEST} , by the effective specimen length of 1.35 m, and the corresponding value calculated with the

code, M_R^{EC4} , using the yield steel strength, f_y , defined in Table 6. Regarding the concrete compressive strength, f_c , the material properties defined in Section 2.2.3 were used. No material partial safety factors were employed in the application of Eurocode 4. Table 15 summarizes the aforementioned design accuracy assessment. Despite exceeding the d/t limit of Eurocode 4, the flexural capacity of both CR-219-3 specimens was evaluated using the calculation procedure presented in Section 4.1 of this paper.

The analysis of the results presented in Table 15 reveals that Eurocode 4 is conservative in predicting the bending capacity of both CFST and RuCFST specimens, in agreement with previous conclusions by other authors, as already stated in the introduction of this paper. It is important to note that, not only does the code lead to conservative predictions for both CR-219-3 specimens, but also that the ratio between the capacity estimated with Eurocode 4 and the actual capacity measured in the tests is similar for all members, including those that violate the cross-section slenderness limit specified in Eurocode 4. This indicates that, although the code may imply that local buckling effects may be relevant for these two specimens, the influence of this effects on the flexural capacity proves to be insignificant. This observation supports a possible relaxation in the future of the cross-section slenderness limits defined in Eurocode 4, eventually through considering a dependence of the slenderness limit as a function of the type of internal forces.

The average difference between the code and the experimental results is around 24%. The confinement effect of the concrete core is only relevant in the case of member compression loading hence its use according to the code is only allowed for values of $e/d \leq 0.1$. Considering that the concrete core is fully compressed only in compression loading one can disregard this concrete behavioural enhancement as the main reason behind the presented conservative differences. However, numerical analysis indicates that the multiaxial stress state developing in the steel tube may contribute to an overall increase of the strength of the member. Additionally, the hardening properties of the steel may also have an important contribution to the reported differences, since, in accordance to the European standard, the yield stress of the steel was used. If the ultimate steel stress was used, the average difference would reduce to 9%. Finally, the high variability of the real steel tube thickness, reported in Section 2.2.1, can also play an important role in these conclusions, particularly in the case of monotonic tests, where cross-section asymmetry can amplify the member bending capacity in comparison to a specimen with an average thickness, if the right alignment conditions are met.

All things considered, one can conclude that the applicability of Eurocode 4 to the design of RuCFST members is valid. Despite the differences in the mechanical properties of the concrete core materials, the design assumptions of the code in the context of this type of columns seem to be solid.

5. Conclusions

In this paper, an experimental assessment of the flexural behaviour of a considerable number of specimens of rubberized concrete filled

Table 15
Comparisons of member bending capacity.

Specimen	F_u^{TEST} [kN]	M_u^{TEST} [kNm]	M_R^{EC4} [kNm]	M_R^{EC4}/M_u^{TEST}
CR-RuC15%-219-3-0%-M	47.8	64.5	48.7	0.75
CR-RuC15%-219-3-15%-M	54.8	74.0	53.8	0.73
CR-RuC15%-219-5-0%-M	89.1	120.2	93.9	0.78
CR-RuC15%-219-5-15%-M	99.7	134.6	98.3	0.73
CR-RuC5%-219-5-0%-M	94.8	127.9	99.0	0.77
CR-RuC5%-219-5-15%-M	103.1	139.1	106.9	0.77
CR-StdC-219-5-0%-M	96.5	130.3	101.6	0.78
CR-StdC-219-5-15%-M	105.3	142.2	111.4	0.78
			μ	0.76
			σ	0.023

circular steel tube members was achieved. The following conclusions can be drawn:

- The newly developed box testing mechanism performed very well throughout the test campaign, proving to be a noteworthy alternative to the traditional test setup;
- Infilling the steel tube with concrete not only improves the bending capacity of the member, but also significantly enhances its ductility;
- Circular CFST and RuCFST test specimens exhibited a very ductile behaviour, both under monotonic and cyclic loading;
- No significant loss of bending capacity was observed in the monotonic tests. In the cyclic tests, some load degradation was detected due to pronounced local buckling developing on the specimens;
- Specimens tested in simple bending and with cyclic lateral loading showed failure of the steel tube due to very prominent local buckling in the specimen's base;
- The concrete type has not a relevant influence on specimen behaviour;
- Loading type effect in simple bending tests shows an influence of more pronounced base local buckling in cyclic loading, as the observed peak lateral load is lower than in the monotonic counterpart;
- Based on the limited number of test results, it was found that cross-section slenderness ratio does not greatly influence both the monotonic and cyclic behaviour of the specimens, considering the d/t values of 73.0 ($C219 \times 3$) and 43.8 ($C219 \times 5$) involved in this study. Although this reflects the considerable ductility of circular CFST members in comparison with other cross-section types, additional monotonic and cyclic tests on CFST members, considering a wider range of d/t and axial load values, should be carried out in order to further validate this conclusion;
- Eurocode 4 is conservative in predicting the bending capacity of the test specimens, yielding on average values of capacity 24% below those measured in the tests. Nonetheless, the differences observed were consistent throughout all the specimens analysed in the study, proving therefore the applicability of the European code to RuCFST members;
- The test results obtained in this research study indicate that the cross-section slenderness limits defined in Eurocode 4 and 8 could be relaxed. This modification could follow the concepts of Eurocode 3 for the classification of non-circular sections, where the plate slenderness limits are dependent on the distribution of normal stresses within the cross-section, i.e., they are dependent on the type of internal forces applied to the cross-section.

Acknowledgments

The authors would like to acknowledge the Portuguese Foundation for Science and Technology (FCT) for the financial support through the research project "Recycling & Seismic Protection: Sustainable High-Performance CFST Columns for Seismic Areas" (PTDC/ECM/117774/2010). Also acknowledged is the support of FERPINTA, by providing all the steel tubes for the experimental campaign, PRESDOURO, for

providing the resources for the casting of the concrete of the specimens, and António Duarte, from IST Lisbon, for his support in the preparation of the RuC mixtures. This work was also supported by FCT, through IDMEC, under LAETA, project UID/EMS/50022/2013.

References

- [1] S. Schneider, Axially loaded concrete-filled steel tubes, *J. Struct. Eng.* 124 (10) (1998) 1125–1138.
- [2] K. Sakino, H. Nakahara, S. Morino, I. Nishiyama, Behavior of centrally loaded concrete-filled steel-tube short columns, *J. Struct. Eng.* 130 (2) (2004) 180–188.
- [3] G. Giakoumelis, D. Lam, Axial capacity of circular concrete-filled tube columns, *J. Constr. Steel Res.* 60 (7) (2004) 1049–1068.
- [4] CEN, EN 1994-1-1 Eurocode 4: Design of Composite Steel and Concrete Structures. Part 1-1, General Rules and Rules for Buildings, European Committee for Standardization, Brussels, Belgium, 2004.
- [5] M. Elchalakani, X.L. Zhao, R. Grzebieta, Concrete-filled circular steel tubes subjected to pure bending, *J. Constr. Steel Res.* 57 (11) (2001) 1141–1168.
- [6] M. Elchalakani, X.L. Zhao, Concrete-filled cold-formed circular steel tubes subjected to variable amplitude cyclic pure bending, *Eng. Struct.* 30 (2) (2008) 287–299.
- [7] L.H. Han, Flexural behaviour of concrete-filled steel tubes, *J. Constr. Steel Res.* 60 (2) (2004) 313–337.
- [8] A.Y. Jiang, J. Chen, W.L. Jin, Experimental investigation and design of thin-walled concrete-filled steel tubes subject to bending, *Thin-Walled Struct.* 63 (2013) 44–50.
- [9] Z.K. Khatib, F.M. Bayomy, Rubberized Portland cement concrete, *J. Mater. Civ. Eng.* 11 (3) (1999) 206–213.
- [10] J. Xue, M. Shinozuka, Rubberized concrete: a green structural material with enhanced energy-dissipation capability, *Constr. Build. Mater.* 42 (2013) 196–204.
- [11] A.P.C. Duarte, B.A. Silva, N. Silvestre, J. de Brito, E. Júlio, J.M. Castro, Tests and design of short steel tubes filled with rubberized concrete, *Eng. Struct.* 12 (2016) 274–286.
- [12] A.P.C. Duarte, B.A. Silva, N. Silvestre, J. de Brito, E. Júlio, J.M. Castro, Experimental study on short rubberized concrete-filled steel tubes under cyclic loading, *Compos. Struct.* 136 (2016) 394–404.
- [13] A.P.C. Duarte, B.A. Silva, N. Silvestre, J. de Brito, E. Júlio, J.M. Castro, Finite element modelling of short steel tubes filled with rubberized concrete, *Compos. Struct.* 2016, <http://dx.doi.org/10.1016/j.compstruct.2016.04.048>.
- [14] CEN, EN 1993-1-1 Eurocode 3: Design of Steel Structures. Part 1-1, General Rules and Rules for Buildings, European Committee for Standardization, Brussels, Belgium, 2005.
- [15] CEN, EN 1998-1 Eurocode 8: design of structures for earthquake resistance, Part 1, General Rules, Seismic Actions and Rules for Buildings, European Committee for Standardization, Brussels, Belgium, 2004.
- [16] A.Y. Elghazouli, J.M. Castro, "Design of Composite Steel/Concrete Structures" in "Seismic Design of Buildings to Eurocode 8", Taylor & Francis, 2009 215–237.
- [17] A. Varma, J. Ricles, R. Sause, L.W. Lu, Seismic behavior and design of high-strength square concrete-filled steel tube beam columns, *J. Struct. Eng.* 130 (2004) 169–179.
- [18] ABAQUS, ABAQUS Documentation, Dassault Systèmes Simulia Corp., Providence, RI, USA, 2011.
- [19] SAC, "Protocol for Fabrication, Inspection, Testing, and Documentation of Beam-column Connection Tests and Other Experimental Specimens", Rep. No. SAC/BD-97, 1997 2.